J Mater Sci (2011) 46:4913–4921
DOI 10.1007/s10853-011-5404-0

Electrical, morphological and structural properties of RF magnetron sputtered Mo thin films for application in thin film photovoltaic solar cells

Guillaume Zoppi · Neil S. Beattie · Jonathan D. Major · Robert W. Miles · Ian Forbes

Received: 21 December 2010 / Accepted: 15 February 2011 / Published online: 2 March 2011

Abstract Molybdenum (Mo) thin films were deposited using radio frequency magnetron sputtering, for application as a metal back contact material in "substrate configuration" thin film solar cells. The variations of the electrical, morphological, and structural properties of the deposited films with sputtering pressure, sputtering power and post-deposition annealing were determined. The electrical conductivity of the Mo films was found to increase with decreasing sputtering pressure and increasing sputtering power. X-ray diffraction data showed that all the films had a (110) preferred orientation that became less pronounced at higher sputtering power while being relatively insensitive to process pressure. The lattice stress within the films changed from tensile to compressive with increasing sputtering power and the tensile stress increased with increasing sputtering pressure. The surface morphology of the films changed from pyramids to cigar-shaped grains for a sputtering power between 100 and 200 W, remaining largely unchanged at higher power. These grains were also observed to decrease in size with increasing sputtering pressure. Annealing the films was found to affect the resistivity and stress of the films. The resistivity increased due to the presence of residual oxygen and the stress changed from tensile to compressive. The annealing step was not found to affect the crystallisation and grain growth of the Mo films.

G. Zoppi (✉) · N. S. Beattie · R. W. Miles · I. Forbes
Northumbria Photovoltaics Applications Centre, Northumbria University, Ellison Building, Newcastle upon Tyne NE1 8ST, UK
e-mail: guillaume.zoppi@northumbria.ac.uk

J. D. Major
Department of Physics, Durham University, South Road, Durham DH1 3LE, UK

Introduction

Molybdenum (Mo) is the most commonly used metal for back contacts in chalcopyrite ($CuInGaSe_2$, CIS)-based thin film solar cells [1]. Other metals can be used [2, 3], however, Mo is the main choice for this application because the Mo layer offers high stability to processing temperature (up to 600 °C) and good adherence to the substrate (which is usually glass) whilst providing a high conductivity and low resistance contact to the CIS absorber layer. Common deposition methods include electron beam evaporation [4, 5] or sputtering, using either a direct current (DC) [3, 6–9] or radio frequency (RF) [10–12] technique. Sputtering, and in particular DC sputtering, has been the method of choice for studying the properties of Mo films since the pioneering work of Scofield [3]. It is also the method which has resulted in the highest solar efficiency [1]. There are fewer reports on RF sputtering and only recently Khatri and Marsillac [10] have performed a limited study of how the Mo properties vary with the deposition parameters; however, the resistivity and stress values achieved were higher than desirable for application in thin film solar cells. As with DC sputtering, RF sputtering parameters such as deposition rate and argon pressure affects lattice stress, crystallographic orientation, electrical, and morphological properties; however, these are also correlated to the deposition system itself. In this study, an in-depth systematic study of how the physical properties of Mo films formed by RF sputtering has been carried out, with the aim of determining which growth parameters control the film

properties, to determine the conditions for producing low resistivity, low stress Mo films, for application in photovoltaic solar cell device structures.

Experimental

Mo thin films were deposited by magnetron RF sputtering onto commercially available soda-lime glass substrates. The substrates of dimensions $76 \times 26 \times 1$ mm^3 were mechanically cleaned in diluted Decon90 solution, rinsed in high purity water and then blown dried in a flow of nitrogen. The depositions took place in a $3 \times 6''$ target magnetron sputter down Nordiko2000 system setup for sequential sputtering using high purity (99.95%) Mo target and argon (99.998% pure) as the sputtering gas. The rotating substrate table was equipped with 4 substrate holders each capable of holding 5 substrates. The base pressure of the vacuum chamber was 5×10^{-7} Torr. The sputtering power was varied from 100 to 900 W and the working pressure from 2 to 22 mTorr. The deposition time was adjusted to yield a film thickness of $\sim$840 nm.

The samples were subsequently annealed at 530 °C for 45 min in a tube furnace evacuated to a primary vacuum level (5×10^{-3} mTorr). The samples were placed in a graphite box to mimic the conditions of selenisation/sulfurisation processes used in the absorber fabrication. Prior to annealing, the tube was backfilled with either high purity argon or forming gas (a 10% mixture H_2 in N_2 gas) to a pressure of 6 and 10 mbar, respectively. The heating and cooling rate were 25 and 2.5 °C/min, respectively. These conditions have previously been used to produce the Mo used to successfully produce thin film solar devices [13, 14].

The structural properties of the deposited layers were analysed using X-ray diffractometry (XRD) using a Siemens D-5000 diffractometer. Scanning electron microscopy (SEM) (carried out using a Hitachi SU-70 SEM) and atomic force microscopy (AFM) (carried out using a Veeco Multimode AFM) were used to assess the morphological properties. The resistivity was determined using a 4-point probe setup (using a Jandel Engineering LTD 4-probe and Keithley 2602 sourcemeter).

Results and discussion

Power density effect

The power applied to the target was varied between 100 and 900 W, while the chamber pressure was maintained at a pressure of 5 mTorr. The deposition time was adjusted between 43 and 580 min to maintain the thickness at 840 ± 20 nm. All films showed good adhesion to the glass substrate, with no delamination observed during further processing or during the tape test [8]. A summary of the electrical and crystallographic properties is shown in Table 1. It can be seen (Table 1 and Fig. 1) that, as expected, the growth rate increases linearly with increasing power. Figure 1 also shows the evolution of the sheet resistance as a function of the sputtering power. For equivalent thickness, the sheet resistance (R_s) of the Mo film decreases sharply when the power is ramped up from 100 to 200 W before decreasing with a much slower rate

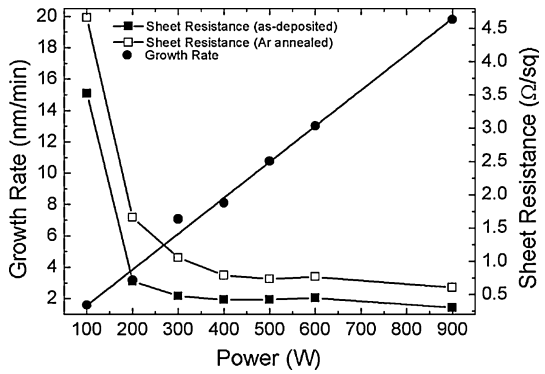

Fig. 1 Growth rate as a function of sputtering power (*filled circle*); sheet resistance as a function of sputtering power (*filled square*) and sheet resistance as a function of sputtering power after annealing at 530 °C for 45 min (*open square*)

Table 1 Properties of as-deposited Mo thin films as a function of sputtering power

Power (W)	Growth rate (nm/min)	Sheet resistance (Ω/□)	Resistivity (μΩ cm)	(110) FWHM (°)	Stress (%)	Grain size (XRD) (nm)
100	1.6	3.52	310	0.494	−0.789	13
200	3.3	0.70	57.1	0.244	0.022	39
300	7.1	0.48	40.4	0.314	0.015	30
400	8.0	0.42	36.2	0.260	0.008	36
500	10.7	0.42	35.4	0.284	−0.004	33
600	13.0	0.45	36.7	0.194	−0.001	45
900	18.6	0.30	23.9	0.222	−0.051	42

for higher sputtering powers. Sheet resistances of less than 0.5 Ω/□ are achieved for sputtering powers greater than 300 W; these are low enough for back contact applications in thin film solar cells. Upon annealing the sheet resistance of the films is increased by a factor of ~2 (Fig. 1). This is due to the formation of a molybdenum oxide layer at the surface of the Mo, due to the Mo at the surface reacting with residual oxygen present in the primary vacuum of the furnace. This would not occur when making solar cells devices because of the presence of additional layers on top of the Mo film during this annealing step.

XRD was used to analyse the crystallographic properties of the deposited films. The inset of Fig. 2 shows a full scan for a typical film. The reflections corresponding to the (110), (211) and (220) planes are detected for diffraction angles of 40.5°, 73.7° and 87.6°, respectively. A fourth reflection at 36.5° is also present but is due to spectral contamination from the beta filter in the XRD setup. Figure 2 shows in detail the (110) reflection, and indicates that the (110) peak intensity decreases with increasing power. More importantly, the peak position shifts as the sputtering power is varied which reflects a change in lattice parameter of the deposit and hence stress, in the films. The detailed position and characteristics of each peak were determined by fitting the data using a Pseudo-Voigt function [15]. From the (110) peak position, the lattice parameter a of the Mo cubic structure was calculated and the relative variation of a compared to the Mo reference lattice parameter $a_0 = 3.1472$ Å [16] yields the extent of stress in the crystal lattice. Negative or positive values can be deduced indicating compressive or tensile stress, respectively. The full width at half maximum (FWHM) of the (110) peak may be used to determine the crystallite size of the structure, via the Scherrer formula [10], as long as the size remains small (<200 nm). The variation of

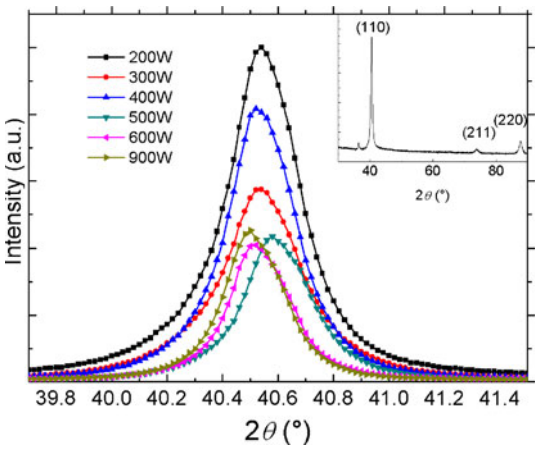

Fig. 2 (110) XRD patterns of Mo films deposited as a function of sputtering power. The *inset* shows a full scan

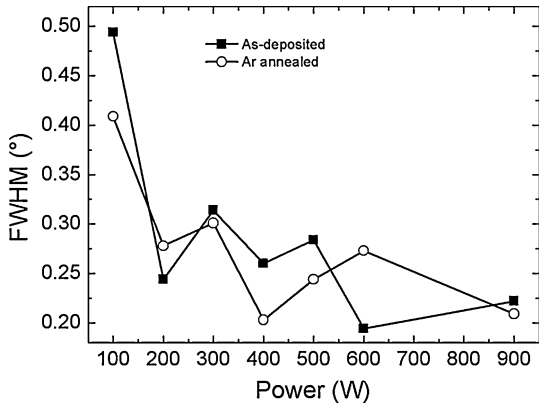

Fig. 3 (110) peak FWHM as a function of sputtering power for as deposited (*filled square*) and argon annealed films (*filled circle*)

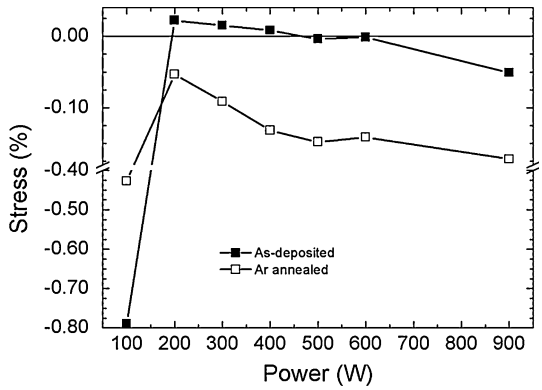

Fig. 4 Lattice stress of Mo films as a function of sputtering power for as deposited (*filled square*) and argon annealed films (*open square*)

FWHM, crystallite size and stress values are shown in Table 1, Figs. 3 and 4. The FWHM of the (110) peak is broadest for the film deposited at 100 W, but it remains relatively invariant for larger powers. The crystallite size varies between 13 and 45 nm but these variations are small between 200 and 900 W. Some fluctuations are observed, but the extent is much less than reported elsewhere [10]. The authors note that the films exhibit tensile stress at low power and this is gradually reduced to become unstressed, or just compressive, for powers greater than 500 W (Fig. 4). It has been suggested that voids, crystallographic impurities, oxygen or argon impurities could be responsible for the stress in the sputtered Mo films. It is argued that these effects are related to the frequency of gas phase collisions in the sputtering system which alters the kinetic energy of both Ar and Mo atoms [3, 10, 17]. At high-deposition powers the energy of the sputtering gas is high resulting in higher deposition rate and the sputtered Mo atoms have high-kinetic energy yielding films with less voids and a lower inclusion of impurities (i.e., Ar or O). This yields a higher conductivity for a higher power and a

reduction of tensile stress. However, as the stress is further reduced for very high power it becomes compressive as the compressive atom peening exceeds the intra-grain tensile forces. This trend is broken when the power is reduced to 100 W and this is due in part to the film becoming more amorphous; however, the reason for this is not fully known. Overall the stress levels measured are very small, at least an order of magnitude smaller than those reported by Khatri [10].

The effects of post growth heat treatment, using an annealing temperature of 530 °C and annealing time of 45 min in 6 mbar Ar atmosphere, on the FWHM and stress values are shown in Figs. 3 and 4. No substantial change is observed in the FWHM values (Fig. 3) indicating no grain evolution under those annealing conditions. The effect on the lattice structure is more pronounced (Fig. 4). Upon heating compressive stress is introduced in all films. The recrystallization temperature of Mo is >900 °C and therefore very little change in structural and electrical properties would be expected at temperatures below 650 °C [18]. However, the soda-lime glass substrate has an annealing point and strain point of 546 and 511 °C, respectively, according to various manufacturers. These temperatures are close to the experimental heat treatment temperature of 530 °C used in this study, which when associated with the thermal expansion of the glass, the authors believe this is the reason of the variations of stress in the Mo films following annealing. At 530 °C the glass starts to soften allowing the Mo film to relax. The thermal expansion of the substrate at this temperature is as much as 0.4% of its length therefore during the slow cool down of the heat treatment the contraction of the glass yields compressive stress in the Mo film.

In order to study the effects of the growth conditions on texture and preferred orientation of the Mo film samples, the texture coefficients C_{hkl} [19] were studied where

$$C_{hkl} = \frac{\frac{I_{hkl}}{I_{r,hkl}}}{\frac{1}{n}\sum_{n}\frac{I_{hkl}}{I_{r,hkl}}} \quad (1)$$

and n is the number of reflections, I_{hkl} the intensity of the hkl reflection and $I_{r,hkl}$ the intensity of the hkl reflection for a completely random sample. Hence C_{hkl} gives a measure of the enhancement of the hkl reflection in comparison to a completely randomly oriented sample. The preferred orientation of each film, as a whole, was analysed from the standard deviation σ of all C_{hkl} values as compared with randomly oriented samples as:

$$\sigma = \sqrt{\sum \frac{1}{n}(C_{hkl} - 1)^2} \quad (2)$$

σ values are used to compare the degree of orientation between different samples, so that lower σ values indicate more randomly oriented samples. For a completely randomised sample the C_{hkl} coefficients would be 1 and the preferred orientation 0 while for a fully aligned sample the C_{hkl} would be 3 for that particular direction and 0 for the others and the degree of preferred orientation 1.4. The variations of texture coefficients are shown in Table 2.

Table 2 Texture coefficients and degree of preferred orientation for as-deposited and argon annealed Mo films

Power (W)	As-deposited				Argon annealed			
	C_{110}	C_{211}	C_{220}	σ	C_{110}	C_{211}	C_{220}	σ
100	2.59	0.41	0.00	1.14	2.56	0.44	0.00	1.11
200	2.44	0.01	0.54	1.04	2.42	0.02	0.56	1.03
300	2.44	0.03	0.53	1.04	2.41	0.04	0.55	1.02
400	2.43	0.03	0.54	1.03	2.31	0.16	0.53	0.94
500	2.36	0.11	0.53	0.98	2.38	0.10	0.53	0.99
600	2.37	0.14	0.49	0.98	2.42	0.04	0.54	1.03
900	2.30	0.18	0.52	0.93	2.28	0.20	0.52	0.92

The data indicates a strong preferred orientation in the (110) direction for all samples. However, as the power is increased a slight loss of this preferred orientation is observed via a decrease in the values of C_{110} and σ. Meanwhile C_{211} and C_{220} values increase and decrease, respectively, indicating a slight shift of orientation from (110) into the (211) direction. The sample deposited at 100 W is anomalous in this respect as the (110) peak is the smallest and broadest for any of the samples in this set, whilst the (220) peak is hardly visible, indicating very small grained structure with a stronger orientation in the (211) direction. The authors believe this indicates why the electrical and lattice properties of this 100 W film are significantly different from the other deposition powers used. Following annealing at 530 °C for 45 min no change is observed in the crystallite orientation and the films remains strongly (110) oriented.

The surface topology was observed by both SEM and AFM. Figure 5a–e shows the AFM micrographs for films deposited between 100 and 900 W. At 100 W the films show grains with a triangular shape. Between 200 and 600 W the grains have a cigar-shape and are well-orientated. For sputtering power greater than 600 W, the grains do not seem to be as well ordered with variations in size starting to appear. Overall however, very little change in grain sizes is observed between 200 and 900 W and this confirms the XRD data. The films' average roughness is between 6 and 10 nm for all films. Figure 5f shows a SEM cross section view of a film deposited at 300 W. The structure is columnar showing narrow grains extending the full thickness of the films which is typical of a sputtered Mo thin film.

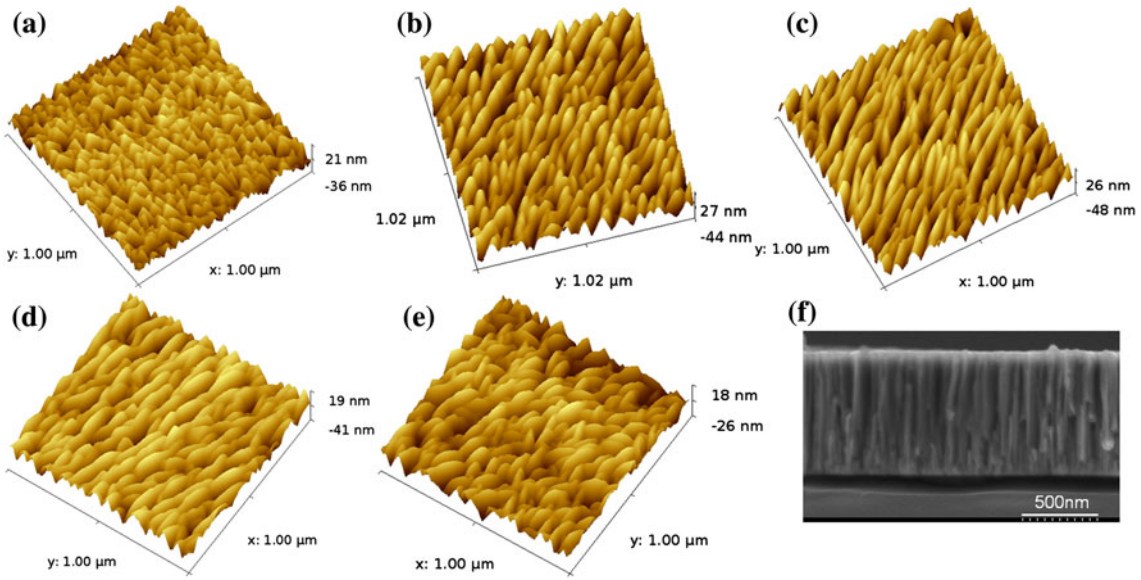

Fig. 5 AFM micrographs for films deposited at (**a**) 100 W, (**b**) 200 W, (**c**) 400 W, (**d**) 600 W, and (**e**) 900 W. (**f**) A cross sectional SEM image of sample deposited at 300 W

Table 3 Properties of as-deposited Mo thin films as a function of sputtering pressure

Pressure (mTorr)	Growth rate (nm/min)	Sheet resistance (Ω/□)	Resistivity (μΩ cm)	(110) FWHM (°)	Stress (%)	Grain size (XRD) (nm)
2.3	6.83	0.260	21.3	0.248	0.046	37.9
5.5	7.00	0.480	40.3	0.314	0.015	30.0
8	7.17	0.616	53.0	0.301	0.081	31.3
12	7.25	0.920	80.0	0.605	0.055	15.5
22	7.33	2.244	197.5	0.720	0.096	13.1

Effect of sputtering pressure

For this study the power and deposition time were fixed at 300 W and 120 min, respectively. The chamber pressure was altered by keeping the gas flow constant and varying the pumping speed. The properties for the as-deposited films are summarized in Table 3. The growth rate is increased nonlinearly with pressure (Fig. 6), giving a variation of 60 nm in thickness between extreme deposition conditions for a given deposition time. Under these conditions the variations in thickness have no noticeable effect on the film properties. The variations of sheet resistance versus chamber pressure are also shown in Fig. 6, with higher sheet resistance being measured for films deposited at higher pressure. This trend is in good agreement with other published data [3, 10].

The electrical properties of the films following post-deposition annealing (530 °C, 45 min) in argon or forming gas (H_2N_2) ambient are also shown in Fig. 6. Following either of the heat treatments the sheet resistance values doubled for all but the lowest pressure sample. There is therefore no influence of the annealing gas ambient on the electrical properties of the films. As described in the previous section this is due to the formation of Mo oxides at the surface during the annealing process.

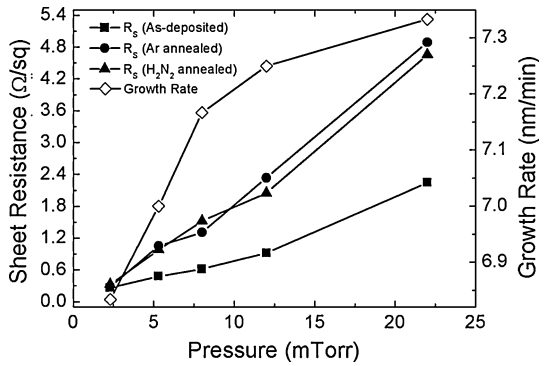

Fig. 6 Growth rate versus sputtering pressure (*open diamond*) and sheet resistance versus sputtering pressure for as-deposited layers (*filled square*), argon annealed (*filled circle*) and forming gas annealed (*filled triangle*) Mo thin films

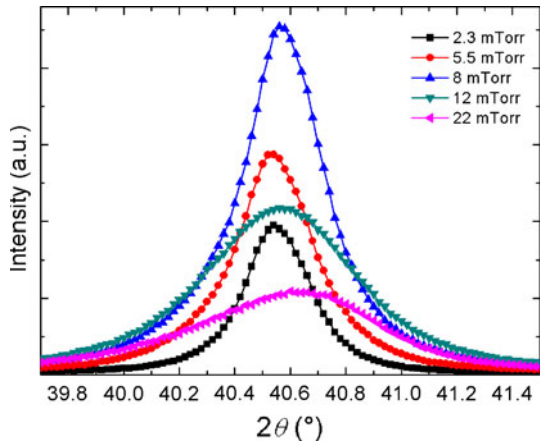

Fig. 7 XRD patterns of Mo films deposited as a function of sputtering pressure

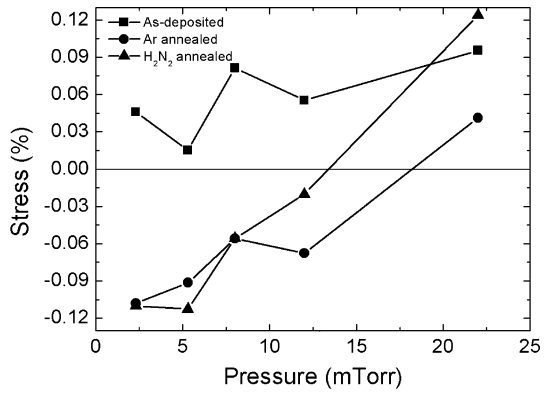

Fig. 8 Evolution of the lattice stress as a function of deposition pressure for as deposited films (*filled square*), argon annealed (*filled circle*) and H_2N_2 annealed (*filled triangle*) films

The XRD spectrum around the (110) peak is shown in Fig. 7. The (110) peak intensity increases when the pressure is increased from 2 to 8 mTorr, but for higher pressure values the peak becomes smaller and broader. This reflects an increase in crystallite size when the pressure is increased from 2 to 8 mTorr; however, beyond ~10 mTorr, this effect is lost and the structural quality degrades. The stress and FWHM values calculated from the (110) XRD data are shown in Figs. 8 and 9, respectively. Overall the stress

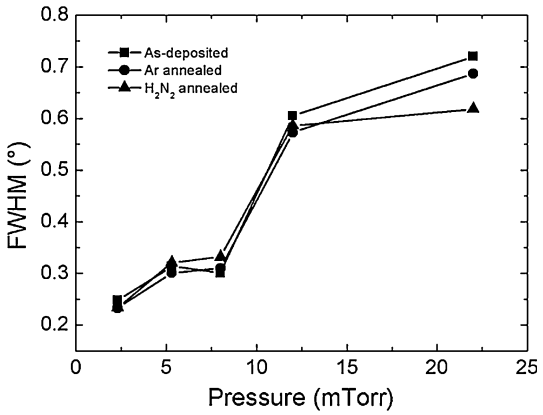

Fig. 9 Evolution of the (110) FWHM as a function of deposition pressure for as deposited film (*filled square*), argon annealed (*filled circle*) and H_2N_2 annealed (*filled triangle*) films

measured is tensile in all cases, less than 0.1% compared to an unstressed film for as-deposited films and decreases for lower deposition pressure. Broader (110) peaks are observed for films deposited at higher pressure (Fig. 9), meaning that the crystallite size of grains orientated in the (110) direction is decreased as the deposition pressure is increased (see also Table 3). Similarly to the previous section, both stress and sheet resistance data can be linked together with the sputtering pressure and the frequency of gas-phase collisions. When reducing the sputtering pressure, the frequency of gas-phase collisions is also reduced and this in turn increases the kinetic energy of the sputtered Mo atoms and neutral Ar atoms from the plasma. It is suggested that the resulting Mo film structure is denser with less intra-grain voids porous grains [3]. This yields a more conductive film and also a less stressed film as observed in Figs. 6 and 8. For pressures greater than 10 mTorr the concentrations of defects is such that the films show an apparent reduced crystalline quality (Figs. 7 and 9) as indicated by the broader peaks. Upon annealing the stress becomes compressive in all cases except at the highest pressure. The trend as function of gas ambient remains similar to that of the as-grown films, however, it can be observed that the absolute change in stress after

Table 4 Texture coefficients and degree of preferred orientation for as-deposited and annealed Mo films as a function of sputtering pressure

Pressure (mTorr)	As-deposited				Argon annealed				H_2N_2 annealed			
	C_{110}	C_{211}	C_{220}	σ	C_{110}	C_{211}	C_{220}	σ	C_{110}	C_{211}	C_{220}	σ
2.3	2.38	0.09	0.53	0.99	2.37	0.10	0.53	0.98	2.42	0.02	0.56	1.03
5.5	2.44	0.03	0.53	1.04	2.41	0.04	0.55	1.02	2.41	0.04	0.55	1.02
8	2.44	0.01	0.55	1.04	2.42	0.01	0.57	1.03	2.43	0.01	0.57	1.03
12	2.35	0.02	0.64	0.99	2.34	0.01	0.64	0.98	2.37	0.01	0.61	1.00
22	2.37	0.04	0.60	0.99	2.37	0.04	0.59	0.99	2.39	0.04	0.57	1.00

annealing is less for films deposited at higher pressure. Following the above discussion the stress can be associated with the sputtering pressure such that lower deposition pressures yield more densely packed columnar grains towards compressive stress whereas higher pressure tends to form a more porous structure under tensile stress [20, 21]. Therefore, the porous nature of the films deposited at higher pressure allows more "flexibility" in the films and more resilience to the annealing process. No change in FWHM values are observed after annealing, indicating that the Mo films are not subject to any grain growth or recrystallisation during this step. This confirms the previous observation.

The variations of texture coefficients and degree of preferred orientation as a function of sputtering pressure and annealing atmosphere are shown in Table 4. The degree of preferred orientation is greatest for film deposited at pressures of 5.5 and 8 mTorr, however, the change in texturing is marginal for the other pressure values.

The surface topology and morphology, i.e., grains size and shape of the deposited films were studied in detail by SEM and AFM, with micrographs being shown in Fig. 10. It was found that not only the size but the shape is affected by the deposition conditions. At 2 mTorr the grains are the largest and are well ordered. At 5 mTorr some grains present sharp triangular tails, while at 8 mTorr the films become smoother and the grains seem to break down into smaller ones. At 12 mTorr all the grains have pyramidal shapes, whereas at 22 mTorr the structure is the most compact with small bean shape grains.

The AFM images were analysed using the Gwyddion software package to determine the grain size distribution at each deposition pressure. These are shown in Fig. 11 where each distribution has been fitted with a Gaussian to obtain an average which is shown in Fig. 12. From Figs. 11 and 12 it is apparent that the average equivalent grain radius decreases from approximately 29 nm to 20 nm as the pressure increases from 2 to 22 mTorr. This is in reasonable agreement with grain size data obtained from XRD (also shown in Fig. 12). Furthermore, it is also apparent from Fig. 11 that at 22 mTorr the standard deviation of the grain size distribution is smaller than at lower pressures, indicating a greater degree of similarity between grains. The average surface roughness R_a, was also obtained from the AFM data and is shown in Fig. 12. A general trend of increasing surface roughness with pressure was observed between 2 and 12 mTorr. A further increase of 10 mTorr resulted in a decrease in surface roughness to $R_a \approx 6$ nm at 22 mTorr. This is consistent with the observed decrease in standard deviation of grain size distribution at this pressure and suggests a different regime of grain formation.

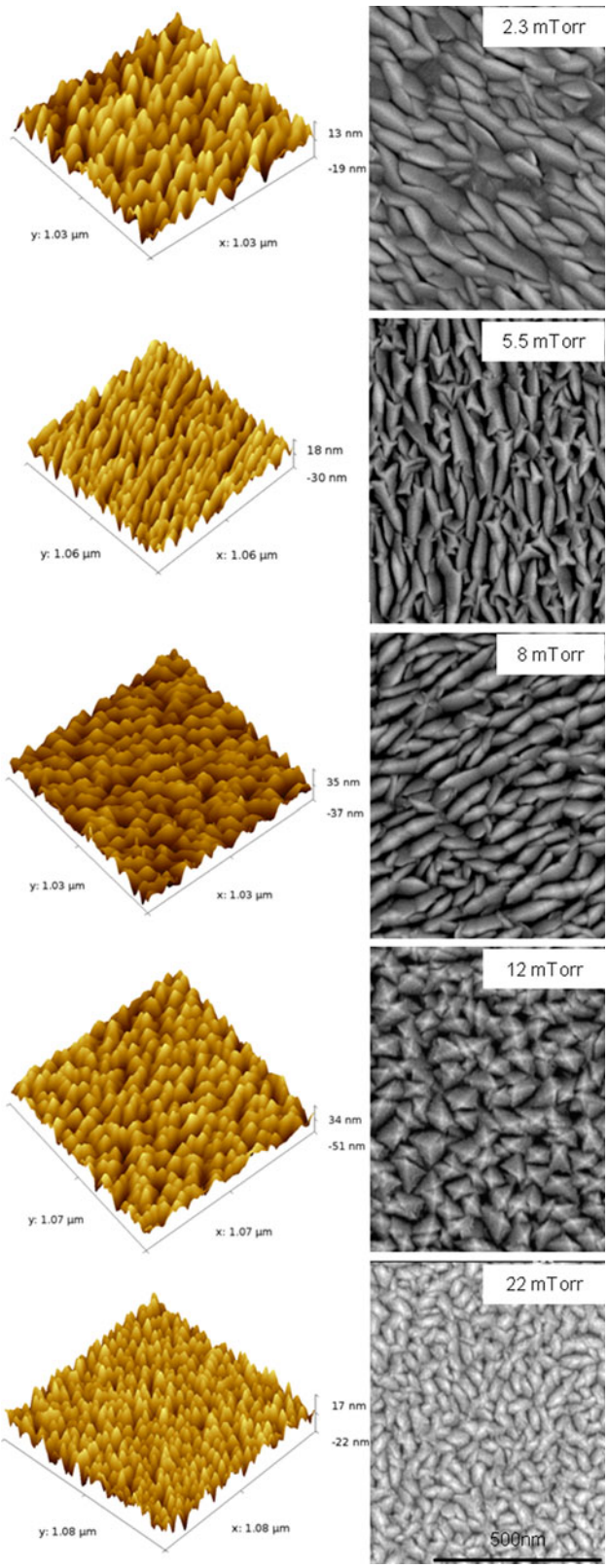

Fig. 10 3D AFM (*left*) and SEM (*right*) micrographs of Mo thin films as a function of deposition pressure

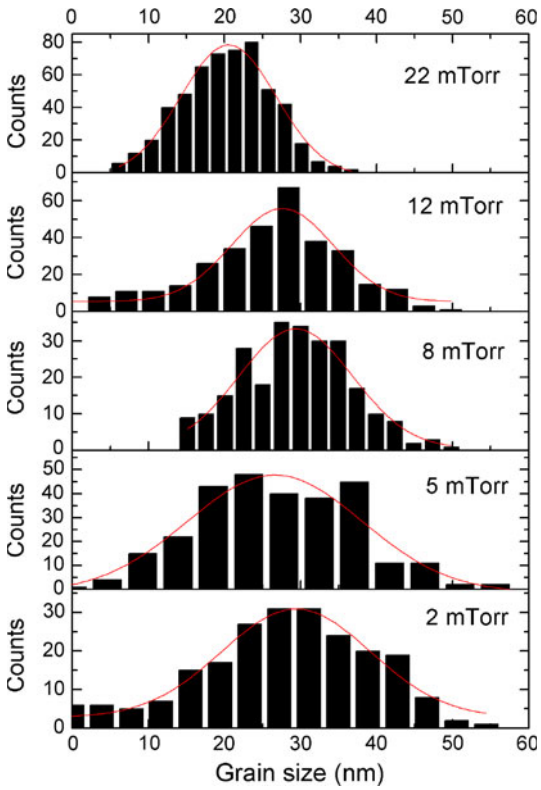

Fig. 11 Grain size distribution as a function sputtering pressure. The data was fitted using a Gaussian distribution

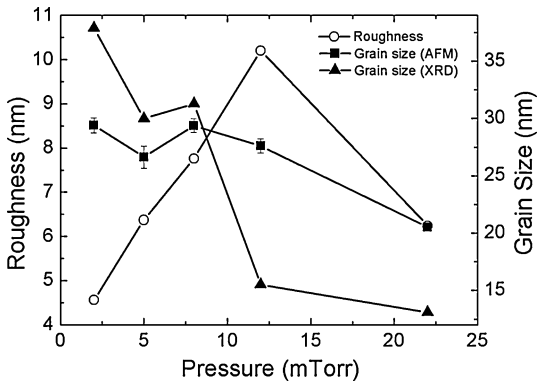

Fig. 12 Roughness (*open circle*) and grain size measurement from AFM images analysis (*filled square*) and XRD measurements (*filled triangle*) as a function of sputtering pressure

This change may be related to increased collisions of Mo atoms with sputtering ions at higher pressure which reduces their kinetic energy and results in more oblique impact angles of incident Mo atoms on the substrate [3].

Conclusions

The electrical, morphological and crystallographic properties of Mo thin films deposited by RF magnetron sputtering have been investigated as a function of sputtering power and pressure. All the films deposited in this study had good adhesion to the substrate regardless of the deposition parameters investigated. The electrical conductivity of the Mo films has been measured to increase with decreasing sputtering pressure and increasing sputtering power. All the films showed a (110) preferred orientation that became less pronounced at higher sputtering power while being relatively insensitive to the process pressure. The lattice stress within the films changed from tensile to compressive with increasing power. The tensile stress increased with increasing sputtering pressure. The grain size and shape remained unchanged for films deposited at sputtering power between 200 and 900 W, whereas grain size decreases with increasing sputtering pressure. Post annealing of the Mo films in argon or forming gas increased the resistivity of the films due to the formation of an oxide layer at the surface and the lattice stress changed from tensile to compressive. From this experiment optimum Mo films properties for thin film solar cell applications are achieved for sputtering power between 300 and 600 W and sputtering pressure around 5 mTorr.

Acknowledgements The authors acknowledge support of the UK Engineering and Physical Sciences Research Council SUPERGEN Initiative for the program 'PV-21'.

References

1. Repins I, Contreras MA, Egaas B, DeHart C, Scharf J, Perkins CL, To B, Noufi R (2008) Prog Photovolt Res Appl 16(3):235
2. Orgassa K, Schock HW, Werner JH (2003) Thin Solid Film 431–432:387
3. Scofield JH, Duda A, Albin D, Ballard BL, Predecki PK (1995) Thin Solid Film 260(1):26
4. Guillen C, Herrero J (2003) J Mater Process Technol 143–144:144
5. Hoffman RA, Lin JC, Chambers JP (1991) Thin Solid Film 206(1–2):230
6. Gordillo G, Grizalez M, Hernandez LC (1998) Sol Energy Mater Sol Cells 51(3–4):327
7. Shen YG (2003) Mater Sci Eng A 359(1–2):158
8. Kadam AA, Dhere NG, Holloway P, Law E (2005) J Vacuum Sci Technol A Vacuum Surf Film 23(4):1197
9. Alleman JL, Althani H, Noufi R, Moutinho H, Al-Jassim M, Hasoon F (2000) In: NCPV program review meeting. Denver, Colorado, p 239
10. Khatri H, Marsillac S (2008) J Phys Condens Matter 20(5):055206
11. Assmann L, Bernede JC, Drici A, Amory C, Halgand E, Morsli M (2005) Appl Surf Sci 246(1–3):159
12. Martinez MA, Guillen C (1998) Surf Coat Technol 110(1–2):62
13. Dale PJ, Samantilleke AP, Zoppi G, Forbes I, Peter LM (2008) J Phys D Appl Phys 41(8):085105
14. Zoppi G, Forbes I, Miles RW, Dale PJ, Scragg JJ, Peter LM (2009) Prog Photovolt Res Appl 17(5):315
15. Vergara L, Olivares J, Iborra E, Clement M, Sanz-Hervás A, Sangrador J (2006) Thin Solid Film 515(4):1814

16. Robbemond A, Thijsse BJ (1997) Nucl Instr Meth Phys Res B 127–128:273
17. Malhotra SG, Rek ZU, Yalisove SM, Bilello JC (1997) J Vacuum Sci Technol A Vacuum Surf Film 15(2):345
18. Schmid U, Seidel H (2005) Thin Solid Film 489(1–2):310
19. Moutinho H, Al-Jassim M, Levi DH, Dippo PC, Kazmerski LL (1998) J Vacuum Sci Technol A16(3):1251
20. Probst V, Rimmasch J, Riedl W, Stetter W, Holz J, Harms H, Karg F, Schock HW (1994) In: Proceedings of 1994 IEEE 1st world conference on photovoltaic energy conversion, New York, p 144
21. Vink TJ, Somers MAJ, Daams JLC, Dirks AG (1991) J Appl Phys 70(8):4301